scientific reports

Check for updates

OPEN

Effect of piston texture at inclination and eccentricity work conditions on damping characteristics of a hydraulic shock absorber

Yangyang Yu[1,2], Junhong Zhang[1,2]✉, Xiangde Meng[2], Dan Wang[2] & Shasha Ma[2,3]✉

In order to accurately predict the damping characteristics of a hydraulic shock absorber under piston inclination and eccentricity conditions, especially, considering effects of piston surface construction. In present work, taking account of piston slight inclination and eccentricity, a more detailed mathematical model was developed to estimate effects of piston texture on damping characteristics. Based on the mathematical models of reservoir and compression stroke coupled with Reynolds equation, a new damping force model was developed, which analyzed effects of piston structure on damping characteristics. The mathematical models of piston texture, piston slight inclination, piston eccentricity and combinations of three cases are developed to analyzed in detailed effects of piston texture at different work conditions on damping characteristics. The results shown that the friction force of piston increases parabolically with increasing depth ratio, and that of piston increases linearly with increasing area ratio. Piston textures have little effects on damping characteristics at specific structural parameters conditions when piston normal operation, however, textures of slight inclined and eccentric piston have great effects. As a result, piston textures might cause high damping force, destroyed comfort and safety. Therefore, it is necessary that effects of piston surface construction were precisely predicted on damping characteristics under different work conditions. The results might provide a new insight for the design of hydraulic shock absorber and investigation of vehicle system dynamics.

Dual-tube hydraulic shock absorber has been widely used in automobile suspension and railway vehicle suspension system[1,2] since the mature technology and moderate cost. The contemporary age, as for automobile and railway vehicle, comfort and safety are paid special attention while pursuing higher velocity. Dynamic damping characteristics of the hydraulic shock absorber have great impact on the dynamic performance of vehicles[3,4]. Dynamic damping characteristics depend on the structure of the shock absorber. However, the structures are designed by the traditional design method including experience, then revised and adjusted by repeating experiments. It will take a long period and high cost. The structures are also designed by numerical simulation method. It is precise, fast, and convenient. However, the shock absorber usually works under complex conditions. It is difficult to obtain precisely damping performance at different complex work conditions. Therefore, it is an important research focus to precisely predict the performance of shock absorber by numerical simulation method to design optimal structures suitable for complex working conditions.

Structures of the shock absorber have great impact on dynamic damping characteristics. Duym[5,6] and Yung[7] established detailed modeling including the internal structure and operation process, analyzed shock absorption performance on internal structure. Besinger[8], Berger[9] and Lion[10] established rheological model including buffer, spring and friction, and analyzed the effect of structural parameters on the damping characteristics. Czop[11] formulated, derived and validated the first-principle non-linear model, investigated structural vibrations on the dynamical interactions between mounting elements, valve systems and the hydraulic actuator of the shock absorber, and captured dynamical characteristic on a wide operating range. Zhang[12] elaborated

[1]State Key Laboratory of Engine, Tianjin University, Tianjin 300354, China. [2]Tianjin Renai College, Tianjin 301636, China. [3]School of Civil Engineering, Tianjin University, Tianjin 300354, China. ✉email: zhangjh@tju.edu.cn; 1218205003@tju.edu.cn

the working principle of membranous dual-cavity based on amplitude sensitive damper (MASD), its dynamic model was derived by combining first-principle modeling of hydraulic components and empirical modeling of membranous valve. At the same time, the influence of the piston and pattern valve construction was analyzed on the dynamic damping. Alireza Farjoud[13] presented nonlinear model of monotube hydraulic dampers, and emphasis on detailed structure of shim stack and their effects on the overall damper performance. Zhou[14] established mechanics model of flexible ring throttle-slice based on elastic mechanical principals. The effect of superposition throttle-slices thickness on throttle opening size was researched in depth. Wang[15] established a new full-parameter model and revealed the nonlinear displacement dependent characteristics of a high-speed rail pantograph dampers. The damping characteristics are analyzed on the internal cross-sections and dimensions of the orifices in the rod by the full-parameter model. Farfan-Cabrera[16] contributed review on the current state and future improvement trends for optimization of critical tribological components which used in vehicles, gave an understanding of the most recent achievements in terms of tribological solutions applied to the critical components. The friction between the piston and cylinder of the hydraulic shock absorber has a critical effect on damping characteristics of the shock absorber, which provides an important direction for the finer and more comprehensive modeling of the shock absorber. Ji[17] and Zhang[18] set up a model on the damping force which considering the friction between the piston and cylinder, analyzed the damping performance of shock absorber. But friction was calculated by a constant or empirical formula, which could not completely reflect the effect of piston structure (including piston surface morphology) on the damping characteristics of the shock absorber.

However, it is lubrication contact between the piston and cylinder of the shock absorber. the effect of surface structures is crucial to the friction performance of lubrication contacts. Especially, the Reynolds equation is widely used to solve friction analysis of the hydrodynamic sliding bearing[19], the piston and cylinder of engine and hydraulic cylinder[20–22], and effect of bearing surface and piston structure could be analyzed on friction in detailed. The condition and principle of dynamic lubrication between piston and cylinder of double-cylinder hydraulic shock absorber are the same as that of dynamic sliding bearing, piston and cylinder of engine and hydraulic cylinder. With the rapid development of vehicle and train, the velocity increases and become higher and higher, the comfort of vehicle and train system becomes more sensitive to parameter variations of component, especially effect of friction on piston surface. Thus, it is imperative to establish more accurate models on the damping characteristics to investigate effect of piston surface structure.

The work conditions of automobile and railway vehicle suspension system are complex and varied. The inclination and eccentricity of the piston are frequently caused under long-term and high-velocity operation, and have great effects on the damping characteristics, causing high damping force to destroy comfort and safety. Wang[23] addressed a more subtle and comprehensive non-linear parametric model of a highspeed rail hydraulic yaw damper, which accurate and robust predicted the damping characteristics with extremely wide velocity range. Alonso[24] dealt with the modelling of yaw dampers and determined the influence of the modelling of this component on the obtained results when predicting the dynamic stability of a vehicle. It was verified that the accurate modelling of the yaw damper is critical when dealing with the vehicle s dynamic performance. Huang[25] set up simplified model of the yaw damper, analyzed its dynamic performance in the range of operating conditions, concluded that the great difference between dynamic and static conditions was caused by the internal damper flexibility under small amplitudes, causing the breakdown occurrence at special working condition or the long-term work. Sun[26] studied distortion characteristics of the shock absorber based on the energy method, obtained that the anti-distortion ability of the shock absorber increases with increasing inflation pressure. The wedge gap between piston and cylinder is generated by inclined and eccentric piston under operating, which caused large friction. Especially, piston surface structure also has great effect on the shape of wedge gap under piston inclination and eccentricity condition, thereby affecting damping characteristics. However, the effects of piston texture on damping characteristics of hydraulic shock absorber under different work conditions are very crucial, which has not been investigated in detail.

In order to investigate the effects of piston surface structure on damping characteristics of shock absorber when the piston is inclined or eccentric, in present work, taking account of piston slight inclination and eccentricity, a more detailed mathematical model is developed to estimate the effect of piston texture on dynamic damping characteristics of shock absorbers. The current work demonstrates the following new contributions: (1) Based on the mathematical models of reservoir and compression stroke coupled with Reynolds equation, a new damping force model was developed, which analyzed effects of piston surface structure on damping characteristics. (2) Damping force was analyzed in detailed under different work conditions including piston texture, piston eccentricity with texture, piston inclination with texture and piston eccentricity plus inclination with texture. (3) With increasing depth ratio δ and area ratio S_p of piston texture, the increasing form of the friction force was investigated. The effect of cylindrical texture on friction force at piston normal operation or inclined and eccentric piston conditions was analyzed. As a result, the results of this study might provide a new insight for the design of hydraulic shock absorber and investigation of vehicle system dynamics.

Simulation model

Figure 1 shows the structural sketch of the double-cylinder hydraulic shock absorber, reflects the work process of extension stroke and compression stroke. The oil passes through the valve system during extension stroke and compression stroke, which produces damping force and reduces vibration energy. The double-cylinder hydraulic shock absorber absorbs the vibration energy.

Extension and compression stroke. The oil passes through the constant orifice and piston gap when the extension valve is not opened. Q_T is the flow rate when the oil passes through the constant orifice of piston assembly. Q_{xl} is the flow rate when the oil passes through the piston gap. Q_T and Q_{xl} are expressed as follows:

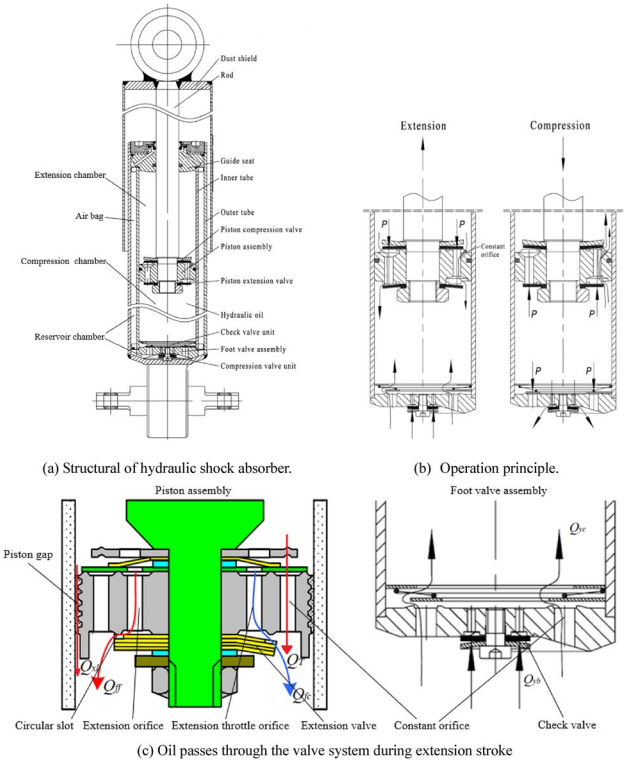

Figure 1. Hydraulic shock absorber.

$$Q_T = C_q A_T \sqrt{\frac{2(P_1 - P_2)}{\rho}} \tag{1}$$

$$Q_{xl} = \frac{2.5\pi d_h h^3 (P_1 - P_2)}{12\mu L_y} \tag{2}$$

where C_q is flow coefficient of the constant orifice of piston assembly, A_T is total area of the constant orifice of piston assembly; ρ is oil density, d_h is piston diameter; μ is dynamic viscosity of the oil; L_y is axial width of piston; h is actual oil film thickness between piston and cylinder; P_1 is the pressure of extension chamber and P_2 is the pressure of compression chamber.

The total flow Q_{fh} of oil from the extension chamber into the compression chamber is expressed as follows:

$$Q_{fh}=Q_T + Q_{xl} \tag{3}$$

Total flow rate Q_{fh} includes flow rate Q_T of the constant orifice of piston assembly, flow rate Q_{xl} of the piston gap and flow rate Q_f of the extension orifice when the extension valve is opened. As shown in Fig. 1c, flow rate Q_f of the extension orifice includes flow rate Q_{fc} of the extension throttle orifice and flow rate Q_{ff} of the circular slot. Q_{fc} and Q_{ff} are in series, thus, $Q_{fc} = Q_{ff}$.

$$Q_{fc} = \varepsilon_{fc} A_{fc} \sqrt{\frac{2(P_1 - P_2)}{\rho}} \tag{4}$$

$$Q_{ff} = \frac{\pi \delta_{rf}^3 (P_1 - P_2)}{6\mu \ln(r_{bf}/r_{kf})} \tag{5}$$

where ε_{fc} is the flow coefficient of extension throttle orifice, A_{fc} is the total area of extension valve orifice, r_{bf} is the outside radius of extension valve plate and r_{kf} is notch radius of the extension valve plate. $\delta_{rf} = f_{rf} - f_{rf0}$, f_{rf} is deformation of extension valve and f_{rf0} is pre-deformation of extension valve.

Flow rate Q_{yc} of the constant orifice of foot valve assembly and flow rate Q_{yb} of check valve are expressed as follow:

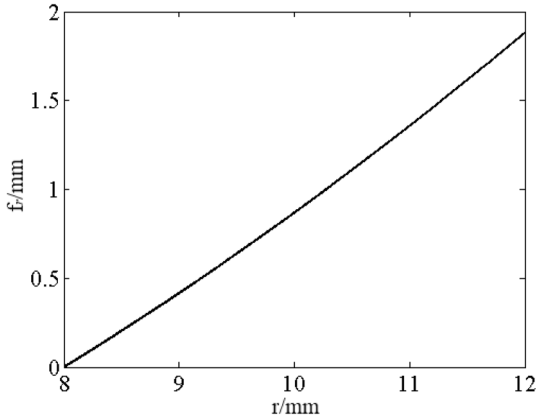

Figure 2. Deformation curve of valve plate.

$$Q_{yc} = \varepsilon_{yc} A_{yc} \sqrt{\frac{2(P_3 - P_2)}{\rho}} \tag{6}$$

$$Q_{yb} = \frac{\pi \delta_{yb}^3 (P_3 - P_2)}{6\mu \ln(r_{bb}/r_{kb})} \tag{7}$$

where ε_{yc} is flow coefficient of the constant orifice of foot valve assembly, A_{yc} is the total area of the constant orifice of foot valve assembly, P_3 is pressure in reservoir chamber, r_{bb} is outside radius of check valve plate and r_{kb} is notch radius of check valve plate.δ_{yb}=$f_{ry} - f_{ry0}$, f_{ry} is deformation of check valve and f_{ry0} is pro-deformation of check valve.

Deformation of valve plate is expressed as follows:

$$f_{rf} = \frac{\Delta P}{h_{ffp}} G_{rffp} \tag{8}$$

where h_{ffp} is the thickness of valve plate and G_{rffp} is the coefficient of valve plate deformation.

Bending deflection of circular disc at arbitrary radius r[14] is expressed as follows, and as shown in Fig. 2.

$$f_r = \frac{P}{h^3} G_r \tag{9}$$

$$G_r = T_{c1} \ln r + T_{c2} r^2 \ln r + T_{c3} r^2 + T_{c4} + T_B r^4 \tag{10}$$

When the extension valve is opened, the total flow rate Q_{fh} of oil from the extension chamber into the compression chamber is expressed as follows:

$$Q_{fh} = Q_T + Q_f + Q_{xl} \tag{11}$$

Total flow rate Q_{yd} of oil from reservoir chamber to compression chamber is expressed as follows:

$$Q_{yd} = Q_{yc} + Q_{yb} \tag{12}$$

Assuming the gas of the reservoir chamber is ideal gas, and the expression can be given as:

$$P_3(t) V(t) = P_{30} V_0 \tag{13}$$

$$V(t) = V_0 + Y A_g \tag{14}$$

where V_0 is initial volume of the gases in the reservoir chamber, P_{30} is initial pressure of the gases in the reservoir chamber, V(t) is the volume of the gases in the reservoir chamber, Y is the relative displacement of piston and A_g is the section area of piston rod.

Assuming sinusoidal excitation is applied to the shock absorber, the relative displacement of the piston is expressed as follows:

$$\begin{cases} Y = Y_0 \sin(\omega t) \\ U = \omega Y_0 \cos(\omega t) \end{cases} \tag{15}$$

The compression stroke is similar to the extension stroke, thus work of compression stroke is not duplicated. The extension chamber pressure P_1, the compression chamber pressure P_2 and the reservoir chamber pressure P_3 are obtained by relationship (13) between oil flow rate passing through the piston assembly and foot valve assembly and piston velocity during extension stroke and compression stroke.

$$\begin{cases} Q_{fh} = U(A_h - A_g) \\ Q_{yh} = U(A_h - A_g) \\ Q_{yd} = UA_g \end{cases} \tag{16}$$

where U is the piston velocity, A_h is cross section area of piston and Q_{yh} is the total flow of oil from the compression chamber into the extension chamber.

Piston/cylinder friction pair lubrication control equation of shock absorber. For a piston of shock absorber under stable working conditions, the two-dimensional Reynolds equation can be expressed in the following form[19]:

$$\frac{\partial}{\partial x}\left(\frac{h^3}{\mu}\frac{\partial p}{\partial x}\right) + \frac{\partial}{\partial \mathrm{y}}\left(\frac{h^3}{\mu}\frac{\partial p}{\partial y}\right) = 6U\frac{\partial h}{\partial x} + 6\frac{\partial h}{\partial t} \tag{17}$$

where p is the oil film pressure at a specific point on the piston surface.

Actual oil film thickness. The expression of actual oil film thickness h between piston and cylinder can be obtained as follows:

$$h = h_0 + \sum_i h_{pi} \quad (i = 1, 2, 3) \tag{18}$$

where h_0 is initial oil film thickness between piston and cylinder and h_{pi} is oil film thickness on outer surface of piston under different cases.

Piston surface has regular shallow texture since machining tolerance and machining precision. Assuming the cylindrical textures are evenly distributed over the piston surface. Figure 3a,b shows schematic of piston textures. Considering piston eccentricity and inclination, Fig. 4 shows schematic of piston textures and the schematic of piston eccentricity and inclination. Figure 5 shows distribution of oil film thickness on the outer surface of the piston under different cases: cylindrical texture (Fig. 5a), piston eccentricity vs. piston eccentricity with texture (Fig. 5b vs. Fig. 5c), piston inclination vs. piston inclination with texture (Fig. 5d vs. Fig. 5e), and piston eccentricity plus inclination vs. piston eccentricity plus inclination with texture (Fig. 5f vs. Fig. 5g). Their oil film thickness h_{pi}[21,27] under different cases are expressed as follows:

$$h_{p1} = \begin{cases} 0 & x^2 + y^2 \le r_p^2 \\ c_0 & x^2 + y^2 \le r_p^2 \end{cases} \tag{19a}$$

$$h_{p2} = e\cos(\theta - \varphi) \tag{19b}$$

$$h_{p3} = \tan\gamma\left(y - \frac{L_y}{2}\right)\cos(\theta - \beta - \varphi) \tag{19c}$$

where e is the eccentricity of central section of piston, θ is the angular coordinate starting from the z axis, φ is the angle between OE_2 and the z axis, γ is angle of the piston inclination and β is the angle between OE_2 and E_1E_3.

Boundary conditions. The flow field between piston and cylinder is a convergent lubrication gap, the Reynolds boundary is applied in the piston modelling process. The effect of cavitation is not included in the analysis, either in terms of the single-phase analysis used or in the application of the boundary conditions, which is considered in the analysis of the piston[20,21]. P_0 is the atmosphere pressure. The boundary conditions are expressed as follows:

$$p(x, y = 0) = P_1, \quad p(x, y = L_y) = P_2, \quad p(x = 0, y) = P_0, \quad p(x = 2\pi R, y) = P_0 \tag{20}$$

A set of assumptions. The work process of hydraulic shock absorber is a complex nonlinear fluid system. Damping characteristics of the shock absorber are affected by many factors including temperature, oil properties and assembly accuracy of each component, and so on. Some factors are ignored in the detailed mathematical model of investigating damping characteristics, including oil temperature, cavitation, gas, oil compressibility, oil density variation. A set of assumptions are shown as follow:

1. Assuming the solubility of the gas in the oil is ignored, gas does not dissolve in oil. Cavitation also is ignored.
2. Assuming oil temperature is fully dissipated during the shock absorber operation. Oil temperature remains constant. Temperature variation characteristics of oil are ignored. Oil viscosity remains constant. The environment temperature is 20 °C. Assuming the oil temperature and environment temperature are same.
3. Assuming the oil is incompressible. The oil will not vaporize due to temperature.

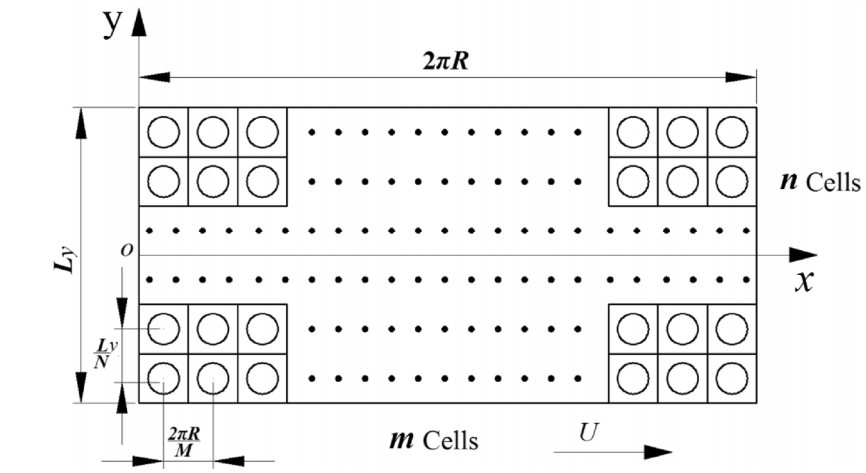

(a) Schematic of the piston surface model (piston texture).

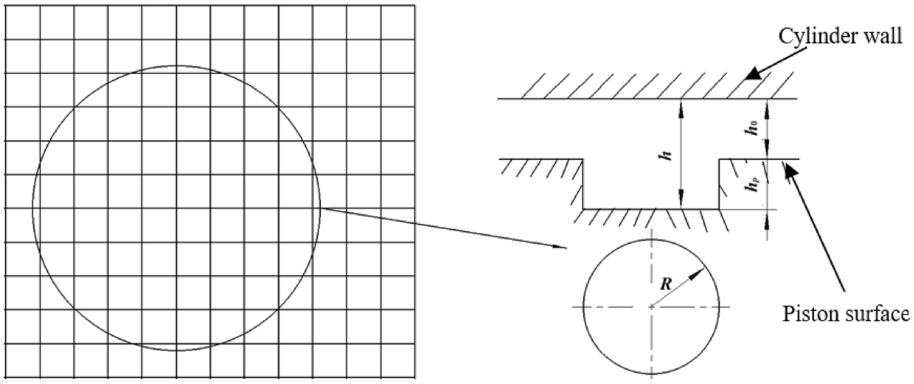

(b) Grid details of cylindrical textures.

Figure 3. Schematic of piston texture.

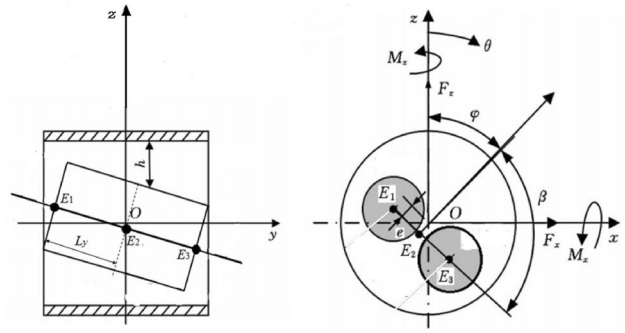

Figure 4. Schematic piston eccentricity and inclination.

4. Assuming the gas of the reservoir chamber is ideal gas, its pressure and volume change in accordance with the laws of thermodynamics.
5. Assuming the oil pressure in each work chamber of the shock absorber is equal, and the pressure varies continuously with the reciprocating motion of the piston in the chamber.
6. All parts of the shock absorber are well assembled.

Numerical solution. In the xOy plane, the piston surface is meshed into m and n grids along the x and y directions. The five-point difference method is used to discrete Eq. (17). The symmetric successive over relaxation (SSOR) method is used to solve the discrete algebraic equation and the pressure p is obtained.

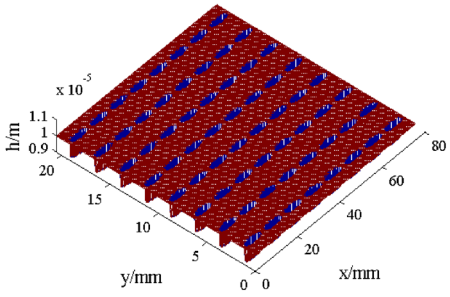

(a) Cylindrical texture.

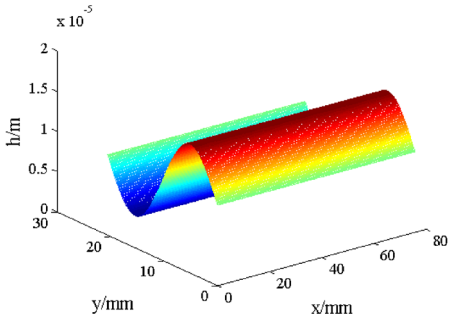

(b) Eccentric.

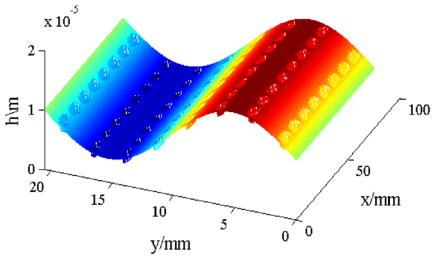

(c) Cylindrical texture and eccentric.

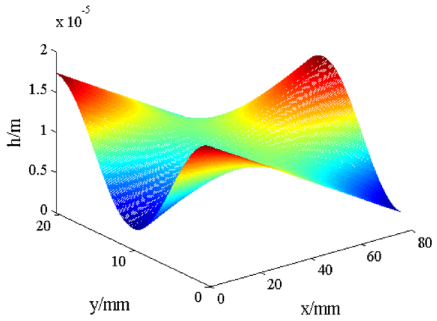

(d)Inclined.

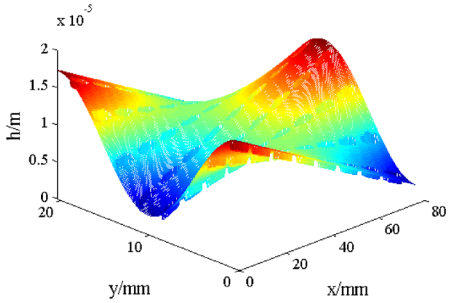

(e) Cylindrical texture and inclined.

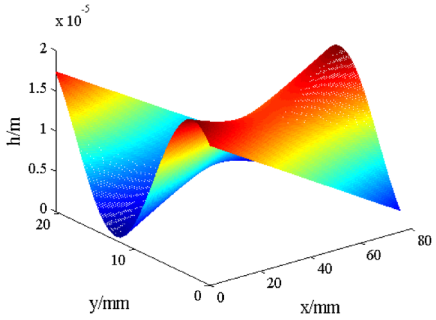

(f)Eccentric and inclined.

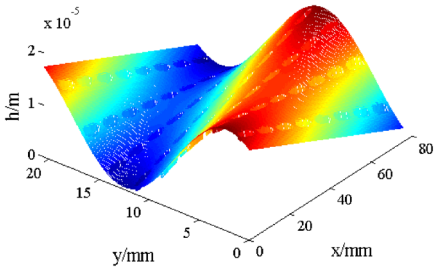

(g) Cylindrical texture, eccentric and inclined.

Figure 5. Distribution of oil film thickness on the outer surface of the piston under different cases.

1. Load capacity

The calculated oil film pressure p is numerically integrated in the whole fluid domain along the x and y directions, and the load capacities W_N can be obtained as follows:

$$W_N = \int_0^{L_x} \int_0^{2\pi R} p dx dy \tag{21}$$

2. Friction force

The calculation of the friction force on the piston is as follows:

$$F_{foil} = \iint_S \left(\frac{h}{2} \frac{\partial p}{\partial x} + \frac{\mu U}{h} \right) \mathrm{d}x\mathrm{d}y \tag{22}$$

Mathematical model of damping force. The dynamic damping characteristics of the shock absorber are mainly determined by the damping force F_f. The damping force F_f is expressed as follows:

$$F_f = P_1(A_h - A_g) - P_2 A_h + F_{foil} \tag{23}$$

where A_h is cross section of the piston, A_g is the section area of piston rod, F_{foil} is film friction force.

The oil film pressures on the outer surface of the piston are calculated under seven different cases of Fig. 5 by solving Reynolds Eq. (17). The pressures distribution on the outer surface of the piston can be obtained in Fig. 6. As a result, the change trend of oil film pressure p and that of actual oil film thickness h are consistent. The high oil film pressures between the piston and the cylinder are induced by increasing or decreasing oil film thickness (forming wedge gap) since wedge effect and extrusion effect. Thus, the friction force F_{foil} of oil film is generated when piston moves.

Results and discussion

The parameters of numerical simulation. The parameters of numerical simulation were provided in the Table 1 and as follow:

As shown in Fig. 7, damping force–displacement loop and damping force–velocity characteristic curve show effects of damping. Maximum damping force F_f is 5559 N.

Effect of depth ratio δ. The depth ratio δ is defined by ratio of texture depth h_p to initial oil film thickness h_0 ($\delta = h_p/h_0$). The friction forces F_{foil} of the cylindrical textured piston are shown by simulating with different depth ratio δ from 0.01 to 0.14 in Fig. 8a. The film friction force F_{foil} of the cylindrical texture increases with increasing depth ratio δ. The friction force F_{foil} of the cylindrical textured piston is 38 N at depth ratio δ of 0.14. The friction force F_{foil} and depth ratio δ shows parabolic curve relationship with increasing depth ratio δ from 0.01 to 0.14. However, as shown in Fig. 8b–e, the effect of friction force F_{foil} since the cylindrical texture on the damping characteristics can be neglected, which is consistent with the results in literature[17]. It also can be seen that the damping force F_f (5600 N) of the shock absorber with cylindrical textured piston increases by 0.74% when depth ratio δ increases to 0.14.

The piston is inclined at an angle of 7.15×10^{-4} rad, the angle β between OE_2 and E_1E_3 is $\frac{\pi}{2}$ rad, the angle φ between OE_2 and Z axis is $\frac{\pi}{2}$ rad. The friction force F_{foil} of the inclined piston and the cylindrical textured inclined piston are shown by simulating with different depth ratio δ from 0.01 to 0.14 in Fig. 9a, the difference ΔF_{foil} of friction force of the cylindrical texture inclined piston and inclined piston are shown in Fig. 9b. The friction force F_{foil} of the cylindrical texture inclined piston increases with increasing the depth ratio δ from 0.01 to 0.14. The friction force F_{foil} of the cylindrical textured inclined piston is higher than that of the inclined piston. The friction force F_{foil} and depth ratio δ shows parabolic curve relationship with increasing depth ratio δ from 0.01 to 0.14. Compared with friction force F_{foil} of inclined piston (101.2 N), when depth ratio δ is increased to 0.14, the difference ΔF_{foil} of friction force is 74.7 N, the friction force F_{foil} of the cylindrical textured inclined piston (175.9 N) greatly increases by 73.81%. However, the effect of friction force since the cylindrical texture inclined piston on the damping characteristics can be neglected in Fig. 9c–f. Compared with the damping force F_f of inclined piston (5661 N), when depth ratio δ is increased to 0.14, the damping force F_f of the cylindrical textured inclined piston (5724 N) greatly increases by 1.11%. As shown in Fig. 9e, the area of damping force–displacement loop slightly increases with increasing depth ratio δ. Thus, effect of the cylindrical textured at inclined piston condition on damping force can be neglected. Compared with the damping force F_f of piston (5559 N), when depth ratio δ is increased to 0.14 and inclined angle is 7.15×10^{-4} rad, the damping force F_f of the cylindrical textured inclined piston (5724 N) greatly increases by 3.02%.

Piston is eccentric, the eccentricity e of the central section of the piston is $0.6h_0$. The friction force F_{foil} of the eccentric piston and the cylindrical textured eccentric piston are shown by simulating with depth ratio δ from 0.01 to 0.14 in Fig. 10a, the difference ΔF_{foil} of friction force of the cylindrical texture eccentric piston and eccentric piston is shown in Fig. 10b. The friction force F_{foil} of the cylindrical texture eccentric piston increases with increasing depth ratio δ from 0.01 to 0.14. The friction force F_{foil} and depth ratio δ shows parabolic curve relationship with increasing depth ratio δ from 0.01 to 0.14. Compared with friction force F_{foil} of eccentric piston (625.8 N), when depth ratio δ is increased to 0.14, the friction force F_{foil} of the cylindrical textured eccentric piston (810.3 N) greatly increases by 29.48%. In Fig. 10c–f, compared with the damping force F_f of eccentric piston (6185 N), when depth ratio δ is increased to 0.14, the damping force F_f the cylindrical textured eccentric piston (6347 N) greatly increases by 0.27%. As shown in Fig. 10e, the area of damping force–displacement loop slightly increases with increasing depth ratio δ. Thus, effect of the cylindrical textured at eccentric piston condition on damping force can be neglected. Compared with the damping force F_f of piston (5559 N), when depth ratio δ is increased to 0.14 and the eccentricity e is $0.6h_0$, the damping force F_f of the cylindrical textured eccentric piston

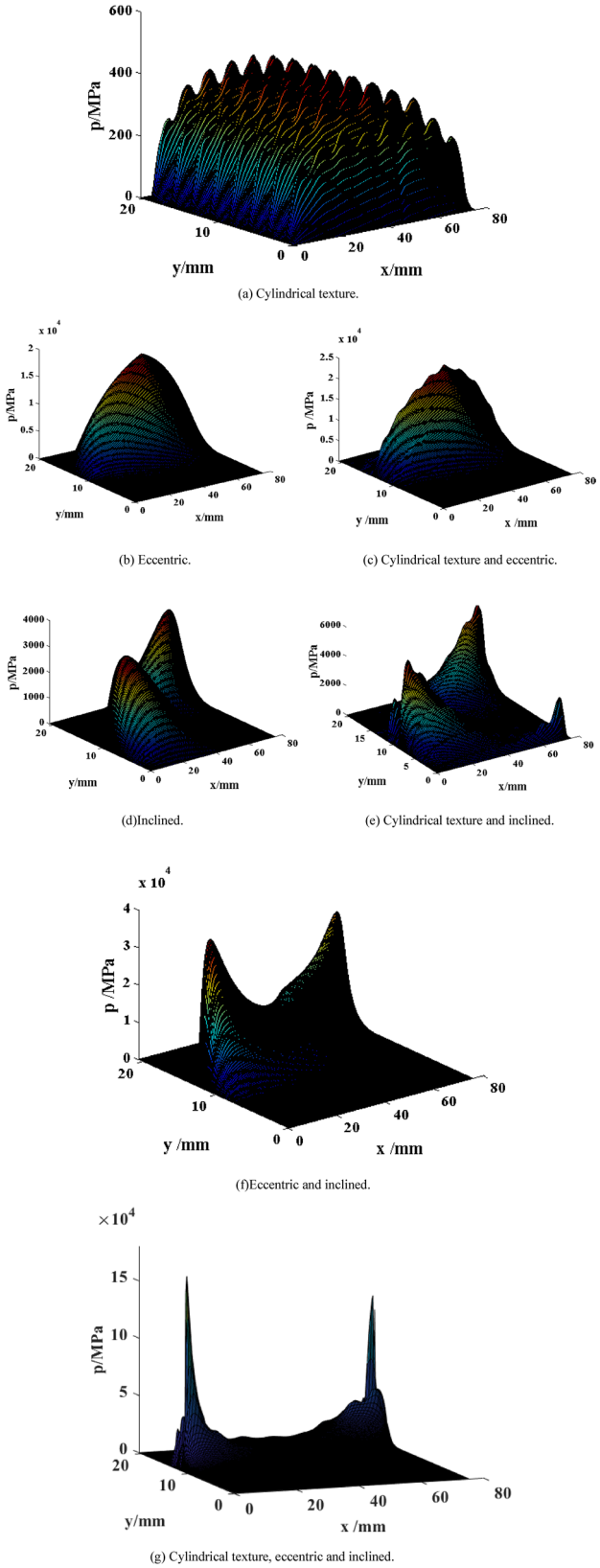

(a) Cylindrical texture.

(b) Eccentric.

(c) Cylindrical texture and eccentric.

(d)Inclined.

(e) Cylindrical texture and inclined.

(f)Eccentric and inclined.

(g) Cylindrical texture, eccentric and inclined.

Figure 6. Distribution of pressure on the outer surface of the piston under different cases.

Parameters	Value
Flow coefficient of the constant orifice of piston assembly C_q	0.82
The constant orifice diameter of piston assembly d_{AT}/mm	0.65
Oil density ρ/kg/m^3	900
Piston diameter d_h/mm	24
Dynamic viscosity of the oil μ/Pa s	0.017
Axial width of piston L_y/mm	20.5
Initial oil film thickness between piston and cylinder h_0/mm	0.01
Flow coefficient of extension throttle orifice ε_{fc}	1
Total area of extension valve orifice A_{fc} /mm^2	1.28
Outside radius of extension valve plate r_{bf} /mm	8
Notch radius of the extension valve plate r_{kf} /mm	5
Flow coefficient of the constant orifice of foot valve assembly ε_{yc}	1
Total area of the constant orifice of foot valve assembly A_{yc} /mm^2	4.05
Outside radius of check valve plate r_{bb}/mm	8
Notch radius of check valve plate r_{kb}/mm	5
Thickness of valve plate h_{ffp}/mm	1.2
Initial volume of reservoir chamber V_0/m^3	0.05×10^{-3}
Initial pressure of reservoir chamber P_{30}/MPa	1
Section area of piston rod A_g/mm^2	78.5

Table 1. Parameters of numerical simulation.

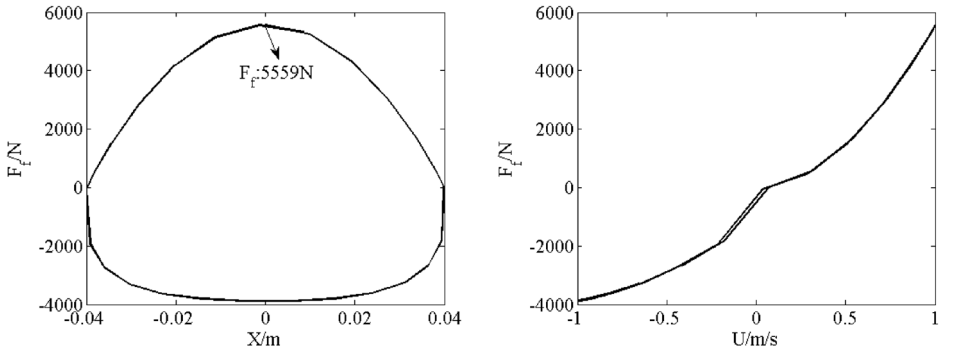

(a) Damping force-displacement loop. (b) Damping force-velocity characteristic curve.

Figure 7. Simulation results of damping characteristic.

(6185 N) greatly increases by 11.26%. As a result, the friction force since the cylindrical texture eccentric piston has great effects on damping characteristics, as shown in Figs. 7c and 10c,d.

Piston is inclined and eccentric. The friction force F_{foil} of the inclined and eccentric piston and the cylindrical textured inclined and eccentric piston are shown by simulating with the depth ratio δ from 0.01 to 0.14 in Fig. 11a. The difference ΔF_{foil} of friction force of the cylindrical texture inclined and eccentric piston and inclined and eccentric piston is shown in Fig. 11b. The friction force F_{foil} of the cylindrical texture inclined and eccentric piston increases with increasing the depth ratio δ from 0.01 to 0.14. The friction force F_{foil} and depth ratio δ shows parabolic curve relationship with increasing depth ratio δ from 0.01 to 0.14. Compared with friction force F_{foil} of inclined and eccentric piston (930.3 N), when the depth ratio δ is increased to 0.14, the friction force F_{foil} of the cylindrical textured inclined and eccentric piston (1682 N) greatly increases by 80.8%. As a result, the cylindrical texture under inclined and eccentric piston condition has great effects on the friction force F_{foil}. As shown in Fig. 11c,d, Compared with the damping force F_f of inclined and eccentric piston (6496 N), when the depth ratio δ is increased to 0.14, the damping force F_f the cylindrical textured inclined and eccentric piston (7123 N) greatly increases by 9.65%. Therefore, it is worth noting that the piston eccentricity plus inclination with cylindrical texture has great effect on damping force. As shown in Fig. 11e,f, the area of damping force–displacement loop increases with increasing depth ratio δ. As shown in Figs. 7 and 11c,d, taking the damping force F_f of piston (5559 N) as the baseline value, when depth ratio δ is increased to 0.14 and the eccentricity e is $0.6h_0$, the damping force F_f of the cylindrical textured inclined and eccentric piston (7123 N) greatly increases by 28.13%. As shown in Figs. 9c,d, 10c,d and 11c,d, it can be concluded that, compared with inclined piston with cylindrical texture or eccentric piston with cylindrical texture, the damping force F_f of the inclined and eccentric pistion with cylindrical textured not only is greater, but also is greater than combination of two situations.

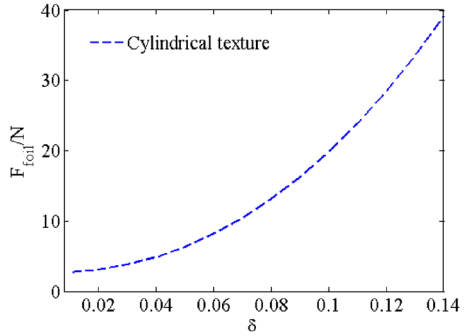

(a) Effect of the depth ratio δ of cylindrical texture on friction forces.

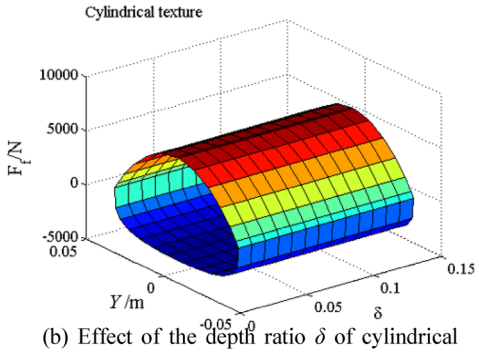

(b) Effect of the depth ratio δ of cylindrical texture on damping force-displacement loop.

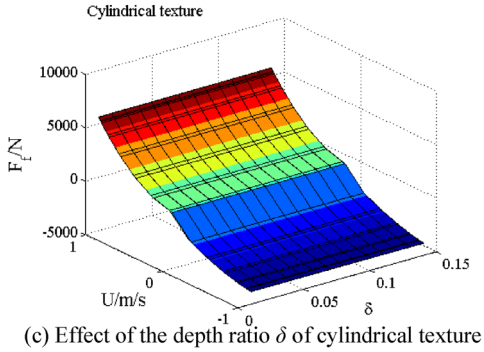

(c) Effect of the depth ratio δ of cylindrical texture on damping force-velocity characteristic curve.

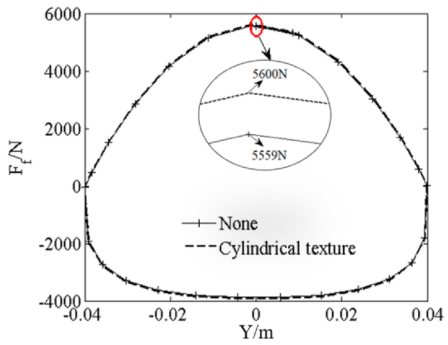

(d) Damping force-displacement loop at depth ratio of 0.14.

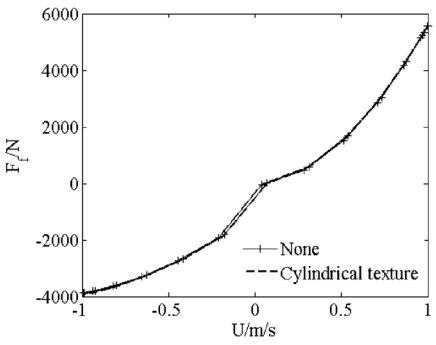

(e) Damping force-velocity characteristic curve at depth ratio of 0.14.

Figure 8. Effect of the depth ratio δ of cylindrical texture on damping characteristic.

Effect of area ratios S_p. The area ratio is defined as $S_p = \frac{4n\pi R_p^2}{2\pi RL_y}$,where n is the number of textures ($n = 16$), R_p is radius of cylinder texture, R is radius of piston. The friction forces F_{foil} of the cylindrical textured piston is shown by simulating with different area ratios S_p from 0.0003 to 0.18 in Fig. 12. The film friction force F_{foil} of the cylindrical texture increases with increasing area ratios S_p from 0.0003 to 0.18, and the friction force F_{foil} of the cylindrical textured piston is 23.8 N at area ratios S_p of 0.18. F_{foil}-S_p curve is approximately linear. However, the effect of friction force since the cylindrical texture on the damping characteristics can be neglected, which is consistent with the results in literature[17].

The piston is inclined at an angle of 7.15×10^{-4} rad, the angle β between OE_2 and E_1E_3 is $\frac{\pi}{2}$ rad, the angle φ between OE_2 and Z axis is $\frac{\pi}{2}$ rad. The friction force F_{foil} of the inclined piston and the cylindrical textured inclined piston are shown by simulating with different area ratios S_p from 0.0003 to 0.18 in Fig. 13a, the difference ΔF_{foil} of friction force of the inclined piston and the cylindrical texture inclined piston is shown in Fig. 13b. The friction force F_{foil} of the cylindrical texture inclined piston increases with increasing area ratios S_p from 0.0003 to 0.18, and the friction force F_{foil} of the cylindrical textured inclined piston is higher than that of the inclined piston. F_{foil}-S_p curves are approximately linear. Compared with friction force F_{foil} of inclined piston (101.2 N), when area

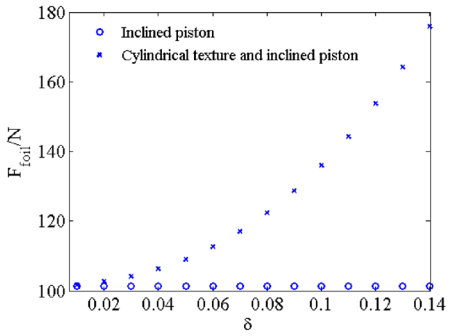

(a) Effect of the depth ratio δ of cylindrical texture at the condition of inclined piston on friction forces.

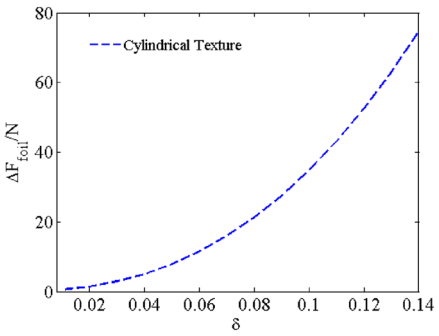

(b) Effect of the depth ratio δ of cylindrical texture at the condition of inclined piston on difference of friction forces.

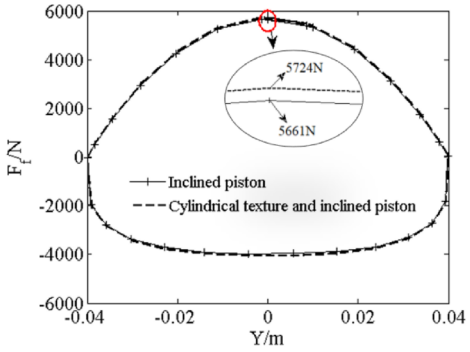

(c) Damping force-displacement loop at the condition of inclined piston.

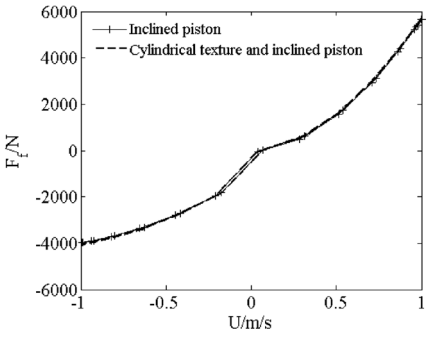

(d) Damping force-velocity characteristic curve at the condition of inclined piston.

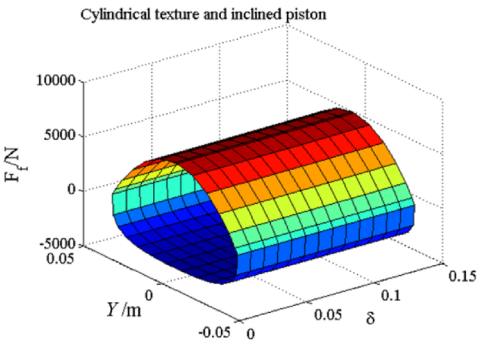

(e) Effect of the depth ratio δ of cylindrical texture at the condition of inclined piston on damping force-displacement loop.

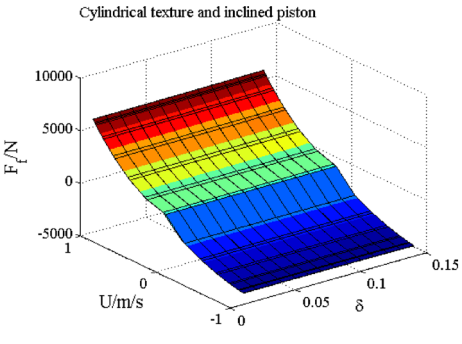

(f) Effect of the depth ratio δ of cylindrical texture at the condition of inclined piston on damping force-velocity characteristic curve.

Figure 9. Effect of the depth ratio δ of cylindrical texture at the condition of inclined piston on damping characteristic.

ratios S_p is increased to 0.18, the friction force F_{foil} of the cylindrical textured inclined piston (154.1 N) greatly increases by 52.27%. The cylindrical textured at inclined piston condition has great effects on friction force. When piston is eccentric, the eccentricity e of the central section of the piston is $0.6h_0$. The friction force F_{foil} of the eccentric piston and the cylindrical textured eccentric piston are shown by simulating with different area ratios S_p from 0.0003 to 0.18 in Fig. 13c, the difference ΔF_{foil} of friction force of the cylindrical texture eccentric piston and eccentric piston is shown in Fig. 13d. The friction force F_{foil} of the cylindrical texture eccentric piston increases with increasing area ratios S_p from 0.0003 to 0.18. F_{foil}- S_p curves are approximately linear. Compared

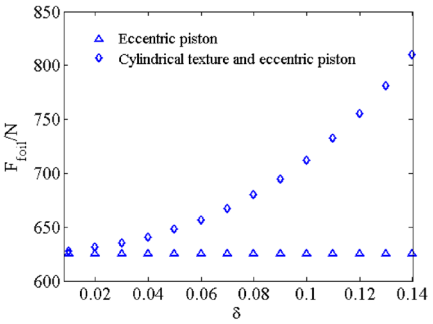

(a) Effect of the depth ratio δ of cylindrical texture at the condition of eccentric piston on friction forces.

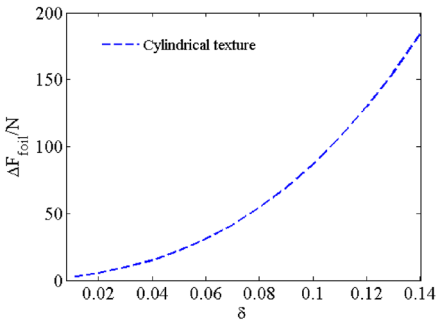

(b) Effect of the depth ratio δ of cylindrical texture at the condition of eccentric piston on difference of friction forces.

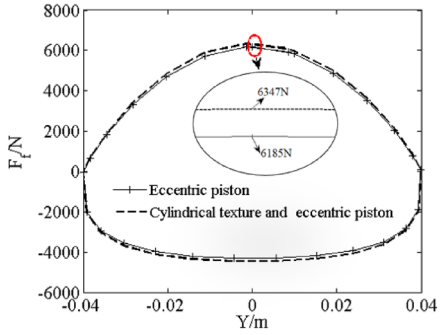

(c) Damping force-displacement loop at the condition of eccentric piston.

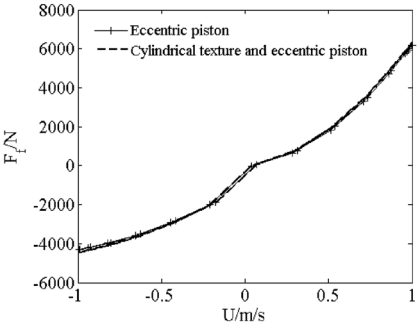

(d) Damping force-velocity characteristic curve at the condition of eccentric piston.

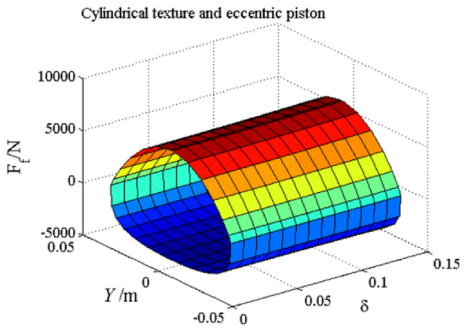

(e) Effect of the depth ratio δ of cylindrical texture at the condition of eccentric piston on damping force-displacement loop.

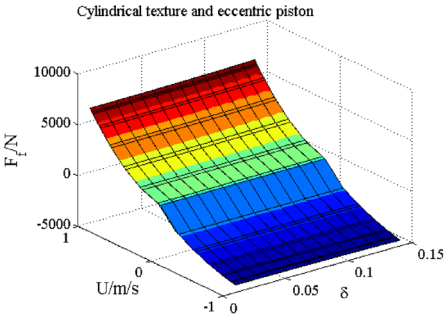

(f) Effect of the depth ratio δ of cylindrical texture at the condition of eccentric piston on damping force-velocity characteristic curve.

Figure 10. Effect of the depth ratio δ of cylindrical texture at the condition of eccentric piston on damping characteristic.

with friction force F_{foil} of eccentric piston (625.8 N), when area ratios S_p is increased to 0.18, the friction force F_{foil} of the cylindrical textured eccentric piston (766.4 N) greatly increases by 22.47%. Thus, the cylindrical textured at eccentric piston condition has great effects on friction force. When piston is inclined and eccentric, the friction force F_{foil} of the inclined and eccentric piston and the cylindrical textured inclined and eccentric piston are shown by simulating with different area ratios S_p from 0.0003 to 0.18 in Fig. 13e, the difference ΔF_{foil} of friction force of the cylindrical texture inclined and eccentric piston and inclined and eccentric piston is shown in Fig. 13f. The friction force F_{foil} of the cylindrical texture inclined and eccentric piston increases with increasing area ratios S_p from 0.0003 to 0.18. F_{foil}- S_p curves are approximately linear. Compared with friction force F_{foil} of inclined and eccentric piston (930.3 N), when area ratios S_p is increased to 0.18, the friction force F_{foil} of the cylindrical

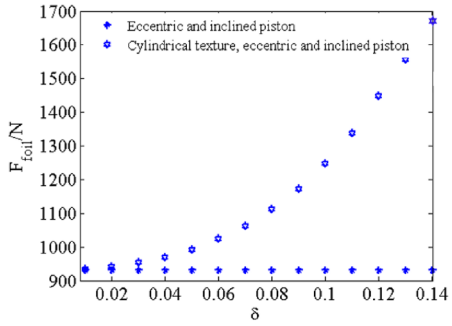

(a) Effect of the depth ratio δ of cylindrical texture at the condition of inclined and eccentric piston on friction forces.

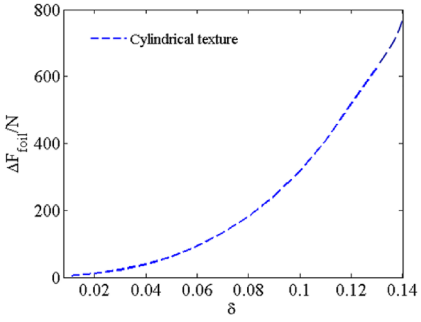

(b) Effect of the depth ratio δ of cylindrical texture at the condition of inclined and eccentric piston on difference of friction forces.

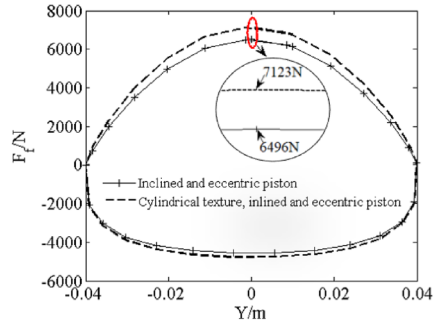

(c) Damping force-displacement loop at the condition of inclined and eccentric piston.

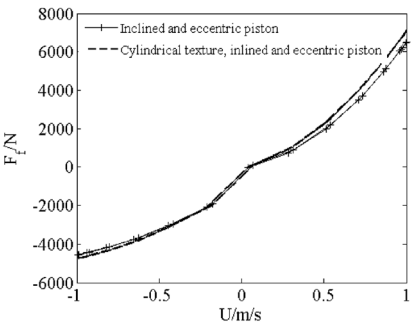

(d) Damping force-velocity characteristic curve at the condition of inclined and eccentric piston.

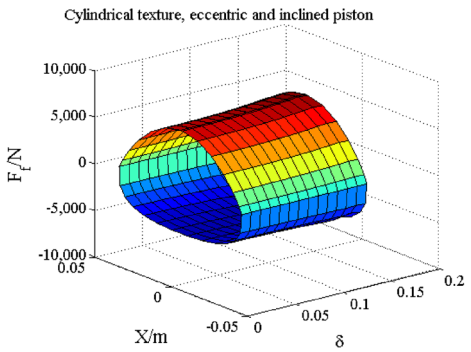

(e) Effect of the depth ratio δ of cylindrical texture at the condition of inclined and eccentric piston on damping force-displacement loop.

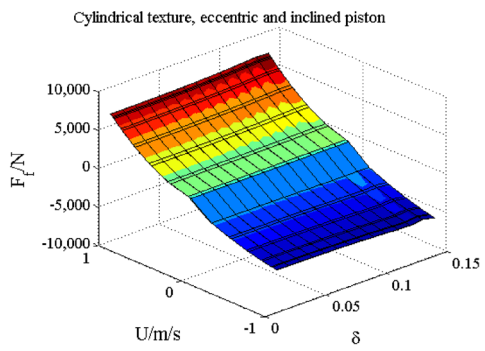

(f) Effect of the depth ratio δ of cylindrical texture at the condition of inclined and eccentric piston on damping force-velocity characteristic curve.

Figure 11. Effect of the depth ratio δ of cylindrical texture at the condition of inclined and eccentric piston on damping characteristic.

textured inclined and eccentric piston (1439 N) greatly increases by 54.68%. As a result, the cylindrical texture at inclined and eccentric piston condition has great effects on the friction force F_{foil}.

As a result, the results of this study might provide a new insight for the design of hydraulic shock absorber and investigation of vehicle system dynamics. Since the upstream and downstream of the piston may change frequently due to the reciprocating motion of the piston, it is necessary to consider the flow conservation law of the lubricant including the cavitation region. Cavitation has great effects on damping characteristics. The disadvantages of these theoretical studies also include the lack of changes in thermophysical properties, primarily the coefficient of dynamic viscosity, from temperature, as well as the determination of temperature changes in the working cavities of the shock absorber. However, it is regrettable that their effects are ignored in this research.

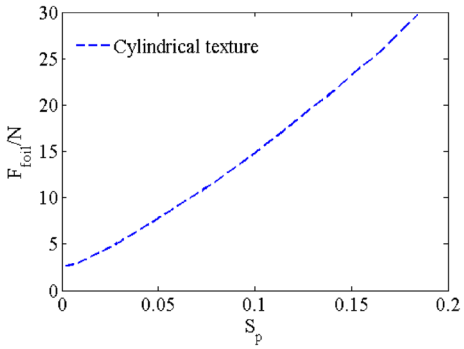

Figure 12. Effect of the area ratio S_p of cylindrical texture on friction forces.

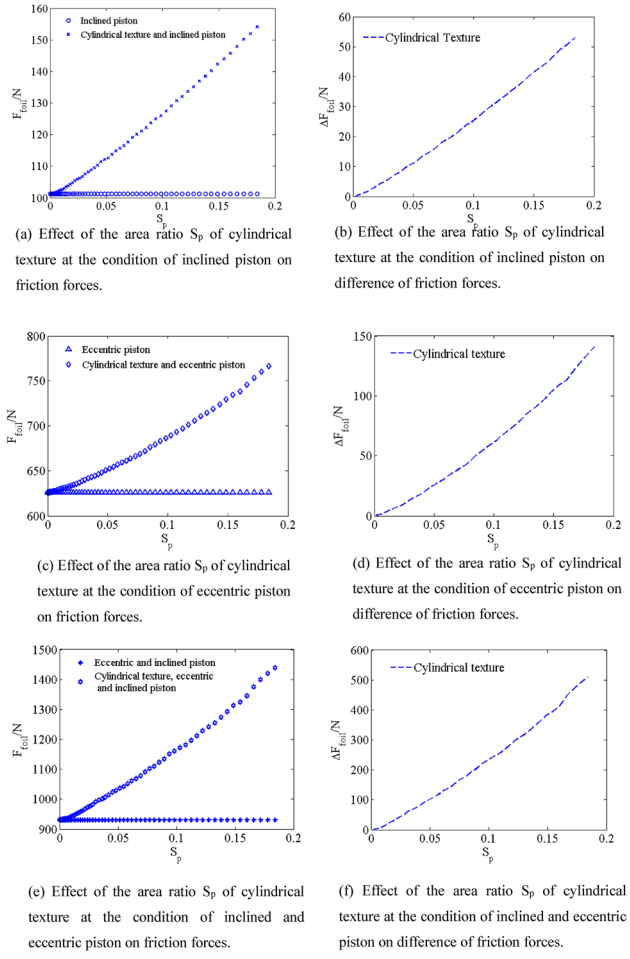

(a) Effect of the area ratio S_p of cylindrical texture at the condition of inclined piston on friction forces.

(b) Effect of the area ratio S_p of cylindrical texture at the condition of inclined piston on difference of friction forces.

(c) Effect of the area ratio S_p of cylindrical texture at the condition of eccentric piston on friction forces.

(d) Effect of the area ratio S_p of cylindrical texture at the condition of eccentric piston on difference of friction forces.

(e) Effect of the area ratio S_p of cylindrical texture at the condition of inclined and eccentric piston on friction forces.

(f) Effect of the area ratio S_p of cylindrical texture at the condition of inclined and eccentric piston on difference of friction forces.

Figure 13. Effect of the area ratio S_p of cylindrical texture at different conditions on friction forces.

The future works should be committed to develop a detail model including oil temperature and cavitation to analyzed more detailed damping characteristics.

Conclusion

In present work, a more detailed mathematical model was developed to estimate the effects of piston texture on damping characteristics of shock absorbers, which taking account of piston slight inclination and eccentricity, and depth ratio δ of piston texture and area ratio S_p of piston texture on friction force and damping characteristics at piston slight inclination and eccentricity conditions were analyzed in detail. The conclusions of current work can be drawn as follow:

1. Based on the mathematical models of reservoir and compression stroke coupled with Reynolds equation, a new damping force model is developed. The mathematical models of piston texture, piston slight inclination, piston eccentricity and combinations of three cases in turn are developed.
2. The cylindrical texture of piston has great effects on the friction force at three different conditions. The friction force of piston increases parabolically with increasing depth ratio δ of piston texture, and that of piston increases linearly with increasing area ratio S_p of piston texture.
3. The cylindrical texture of piston has little effects on damping characteristics at specific structural parameters condition when piston normal operates. The cylindrical texture of piston has great effects on damping characteristics at piston eccentricity and incline condition. The damping force F_f of the cylindrical textured inclined and eccentric piston might greatly increases under certain parameters.

Received: 1 November 2021; Accepted: 26 May 2022
Published online: 13 June 2022

References

1. Yang, M. J., Yu, J. Q. & Guo, Y. B. Present situation and development tendency of shock absorbers in vehicle suspensions. *Eng. Test* **59**(02), 96–103 (2019).
2. Gao, H. X., Chi, M. R., Dai, L. C., Yang, J. G. & Zhou, X. Z. Mathematical modelling and computational simulation of the hydraulic damper during the orifice-working stage for railway vehicles. *Math. Probl. Eng.* 1–23 (2020).
3. Lee, C. T. Study of the simulation model of a displacement sensitive shock absorber of a vehicle by considering the fluid force. *J. Automob. Eng.* **219**(8), 965–975 (2005).
4. Lee, C. T. & Moon, B. Y. Simulation and experimental validation of vehicle dynamic characteristics for displacement sensitive shock absorber using fluid-flow modeling. *Mech. Syst. Signal Process.* **20**, 373–388 (2006).
5. Duym, S. & Reybrouck, K. Physical characterization of nonlinear shock absorber dynamics. *Eur. J. Mech. Environ. Eng.* **43**, 18–188 (1998).
6. Duym, S. Simulation tools, modelling and identification, for an automotive shock absorber in the context of vehicle dynamics. *Veh. Syst. Dyn.* **33**, 261–285 (2000).
7. Yung, V. Y. B. & Cole, D. J. Modelling high frequency force behaviour of hydraulic automotive dampers. *Veh. Syst. Dyn.* **44**, 1–31 (2006).
8. Besinger, F. H., Cebon, D. & Cole, D. J. Damper models for heavy vehicle ride dynamics. *Veh. Syst. Dyn.* **24**, 35–64 (1995).
9. Berger, H. Rheologische Dämpfermodelle für den Einsatz in der MKS-Simulation. Diploma thesis, (Vienna University of Technology, 2002).
10. Lion, A. & Loose, S. A thermomechanically coupled model for automotive shock absorbers: Theory, experiments and vehicle simulations on test tracks. *Veh. Syst. Dyn.* **37**, 241–261 (2002).
11. Czop, P. & Slawik, D. A high-frequency first-principle model of a shock absorber and servo-hydraulic tester. *Mech. Syst. Signal Process.* **25**, 1937–1955 (2011).
12. Zhang, Y., Guo, K., Li, S. E., Xiong, S. & Zheng, M. Prototyping design and experimental validation of membranous dual-cavity based amplitude selective damper. *Mech. Syst. Signal Process.* **76–77**, 810–822 (2016).
13. Farjoud, A., Ahmadian, M., Craft, M. & Burke, W. Nonlinear modeling and experimental characterization of hydraulic dampers: Effects of shim stack and orifice parameters on damper performance. *Nonlinear Dyn.* **67**, 1437–1456 (2012).
14. Zhou, C. & Gu, L. Superposition throttle-slices openings size and characteristic test of telescope-damper. *Chin. J. Mech. Eng.* **43**(6), 210–215 (2007).
15. Wang, W., Zhou, Z., Zhang, W. & Iwnicki, S. D. A new nonlinear displacement-dependent parametric model of a high-speed rail pantograph hydraulic damper. *Veh. Syst. Dyn.* **58**(2), 272–289 (2020).
16. Farfan-Cabrera, L. I. Tribology of electric vehicles: A review of critical components, current state and future improvement trends. *Tribol. Int.* **138**, 473–486 (2019).
17. Ji, Y. *Study on the Physical Modeling and Design of Hydraulic Automotive Twin-tube Shock Absorbers*, Vol. 6, 11–21 (Jilin University, 2015).
18. Zhang, K. *Simulation and Experimental Study on Damping Characteristics of Mono-tube Pneumatic Shock Absorber*, Vol. 6, 18–33 (Zhenjiang Jiangsu University, 2016).
19. Wang, J. *et al.* Study on lubrication performance of journal bearing with multiple texture distributions. *Appl. Sci.* **8**, 244 (2018).
20. He, Z. Piston skirt friction loss and dynamic analyses based on FEM method. *Ind. Lubr. Tribol.* **70**(4), 656–672 (2018).
21. Mao, Y., Zeng, L. & Lu, Y. Modeling and optimization of cavitation on a textured cylinder surface coupled with the wedge effect. *Tribol. Int.* **104**, 212–224 (2016).
22. Yu, G., Zeng, L. & Mao, Y. Analysis on hydrodynamic lubrication performance of micro-texture on hydraulic cylinder piston surface. *Mech. Sci. Technol. Aerospace Eng.* **36**(12), 1823–1829 (2017).
23. Wang, W. L., Huang, Y., Yang, X. J. & Xu, G. X. Non-linear parametric modelling of a high-speed rail hydraulic yaw damper with series clearance and stiffness. *Nonlinear Dyn.* **65**, 13–34 (2011).
24. Alonso, A., Giménez, J. G. & Gomez, E. Yaw damper modelling and its influence on railway dynamic stability. *Veh. Syst. Dyn.* **49**(9), 1367–1387 (2011).
25. Huang, C. & Zeng, J. Dynamic behaviour of a high-speed train hydraulic yaw damper. *Veh. Syst. Dyn.* **56**(12), 1922–1944 (2018).
26. Sun, X., Tian, X., Bao, L. & Chen, S. Open valve and distortion characteristics of inflatable damper based on energy method. *Chin. Hydraul. Pneumatics* **09**, 33–37 (2017).
27. He, Z. *et al.* Inter-asperity cavitation for misalignment journal lubrication problem based on mass-conservative algorithm. *Zhejiang Univ.-Sci. A Appl. Phys. Eng* **14**(9), 642–656 (2013).

Acknowledgements

The authors wish to acknowledge the financial support from Scientific and Technological Research Program of Tianjin Municipal Education Commission (2019KJ152) and Tianjin Science and Technology Program Project (20YDTPJC02020).

Author contributions

Y.Y. developed the shock absorber models with textures and conducted the analyses; S.M. wrote the paper; J.Z. contributed analysis tools; X.M. developed the baseline shock absorber model; D.W. revised the paper.

Competing interests
The authors declare no competing interests.

Additional information
Correspondence and requests for materials should be addressed to J.Z. or S.M.

Reprints and permissions information is available at www.nature.com/reprints.

Publisher's note Springer Nature remains neutral with regard to jurisdictional claims in published maps and institutional affiliations.